# Stick–Slip Patterning at Low Capillary Numbers for an Evaporating Colloidal Suspension

Hugues Bodiguel, Frédéric Doumenc, Béatrice Guerrier

# Stick-slip patterning at low Capillary numbers for an evaporating colloidal suspension

Hugues Bodiguel,[*,†,‡] Frédéric Doumenc,[*,†] and Béatrice Guerrier[*,†]

†*UMPC Univ Paris 06, Univ Paris-Sud, CNRS, Lab FAST, Bat 502, Campus Univ, Orsay, F-91405, France.*

‡*current address: Lab LOF, CNRS UMR 5258 - Univ. Bordeaux 1 - IPB - Rhodia, 178 Av. Dr Schweitzer, F-33608 Pessac, France*

E-mail: hugues.bodiguel@u-bordeaux1.fr; doumenc@fast.u-psud.fr; guerrier@fast.u-psud.fr

**Abstract**

Pattern formation from a silica colloidal suspension that is evaporating has been studied when a movement is imposed to the contact line. This article focuses on the stick-slip regime observed for very low contact line velocities. A capillary rise experiment has been specially designed for the observation and allows us to measure the pinning force that increases during the pinning of the contact line on the growing deposit. We report systematic measurements of this pinning force and derive scaling laws when the velocity of the contact line, the colloid concentration, and the evaporation rate are varied. Our analysis supports the idea that the pinning of the contact line results from a competition between the geometry of the growing deposit and the force due to gravity.

# Introduction

The coupling between evaporation and particle deposition has been the focus of numerous studies during the past decade. The idea of taking advantage of evaporation (usually water evaporation) to control the assembly of small particles (from molecules to colloids) on a surface seems to be a promising and rather simple technique. However, controlling all the parameters that govern the coating induced by evaporation remains difficult.

Several types of material have been investigated, colloids including silica particles[1] and polymer beads,[2,3] but also small molecules,[4] carbon nanotubes,[5] polymers[6,7] and biological molecules.[8] If some specific features may appear with evaporation of polymer droplets due to their rheology,[7] the deposition process seems to be generic and to be relatively independent on the nature of the material.[9] It has been shown that several methods could then be used to control the spatial organization of the deposit on a substrate. Using photo-lithography, one can for example design a heterogeneous surface that is able to pin the contact line in the wetting region and thus induces a control deposition of the material.[10,11] Other techniques may consist in using an external field[12] or a local dispense of some small fluid volumes.[13]

The famous coffee stain effect has been explained by Deegan *et al*[14] and it seems rather clear now that it requires the coupling of different phenomena, namely the hydrodynamic flow inside the droplet[15–17] and the ability for the deposit to pin the contact line. The coffee stain effect has been the focus of several experimental studies on the drying of droplets at different length scales,[18–23] and of significant theoretical work.[24–28] Despite the simplicity of those experiments, and the potential applications of evaporating droplets, its physical description remains quite complicated. The drying of a droplet is a non stationary phenomenon since its volume decreases and the non volatile solute concentration increases. Thus, the effects of concentration, droplet volume, and evaporation rate are intertwined, which results in a rather complex physical description of the drying. Simplifications of the physical description are possible if one assumes that the contact line is pinned.[27,28] However, the various experiments and systems exhibit different pinning features, which are either multiple rings,[18] strong

pinning[23] or, in some cases, no pinning.[15] Thus, the coupling between the experimental parameters and the pinning of the contact line needs to be understood.

On the other hand, dip-coating experiments have been also investigated.[29–31] This configuration has of course a direct link to industrial processes in coating technology but is also of great interest for scientific reasons. Indeed, this experimental configuration allows a stationary phenomenon to occur, since the concentration of the liquid bath remains constant, in contrast to the drying of droplets. Moreover, it offers a new experimental parameter that is the velocity at which the plate is withdrawn from the bath. The contact line movement linked to this velocity should allow a competition between particle accumulation, pinning at the contact line and displacement. Thus, one can expect that the dip-coating configuration could help to better describe and control the respective role of the different phenomena that are exhibited in the coffee-stain effect.

In the regime of low capillary numbers, two regimes have been successively observed, depending on the velocity of the plate.[29] At very low velocities, the rate of particle deposition is high enough to produce a macroscopic accumulation and a pinning of the contact line, similarly to experiments on droplets. In this regime, the coating is periodic as a result of successive pinnings. At higher velocities, the deposition appears to be disordered, and, at most, one particle layer is deposited.

Recently we reported some results using a different geometry,[9,32] a capillary rise between two plates. This configuration could be easily compared to the one of the dip-coating experiment, since the main difference is the size of the meniscus. It is fixed by the gap between the plates in our case, whereas it is the capillary length in the dip-coating experiment. We thus expect some similar behavior, that is to say stationary regimes with either periodical patterns at low velocities, either disordered deposition at higher velocities. The capillary rise experiment has two main advantages that are the sensitivity of the experiment to contact line pinning, and a more precise control of the evaporation flux. The former is rather obvious, since decreasing the length scale of the meniscus leads to an increase of the sensitivity

of the contact line position. Our set up is somewhat similar to the one used by Abkarian *et al* who investigated evaporation of a suspension of polystyrene beads inside a tube.[2] The evaporation in the small tubes used could however not be considered steady and the authors hardly found a stationary regime.

In a previous paper the systematic study of the deposit obtained in stationary regimes allowed us to characterize an evaporative regime which is relevant at low velocities.[9] With or without pinning and for different systems, the deposition rate is constant in this regime and does not depend on the contact line velocity. The high sensitivity of the capillary rise experiment already allowed us to measure with sufficient accuracy the pinning force that is responsible for the contact line pinning induced by the colloidal deposit, and then for the formation of regular coated patterns.[32] Our previously reported results indicate that the pinning force is related to the geometry of the deposit, for the system understudy, whatever the exact experimental conditions are (particle volume fraction, evaporation rate, contact line velocity). This result suggests the need for a deeper analysis of the role of these experimental parameters in the formation of the deposit. In the present article, we report pinning force measurements obtained using the same technique, with the three above-cited parameters being varied systematically.

# Experimental details

## Capillary rise

Figure 1 shows the experimental set up. A capillary rise is achieved between two glass plates immersed in a reservoir. The glass plates are 2 mm thick, and their planar dimensions are 5.6 cm $\times$ 8 cm. They are separated by four spacers to ensure parallelism. All the results presented here have been obtained with 1 mm thick spacers. Parallelism of the glass slides has been verified by measuring the capillary rise height as a function of the contact line position. Typical variations are less than 1%, which ensures that a good parallelism is

achieved.

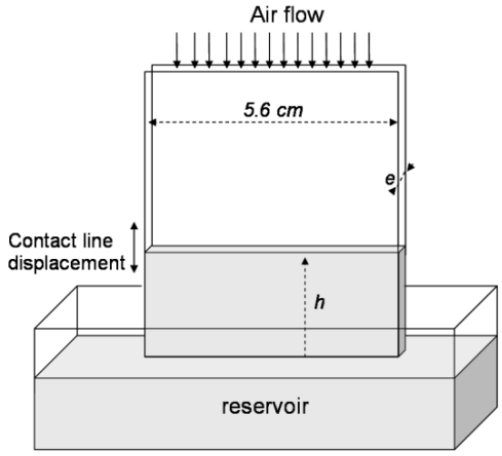


Figure 1: Scheme of the experimental set up. A capillary rise is achieved between two glass slides immersed in a reservoir. A syringe pump (not shown) is used to empty the reservoir and thus to obtain a displacement of the contact line. An air flow is driven between the glass slides.

The planar dimensions of the reservoir are $3\,\mathrm{cm} \times 8\mathrm{cm}$. This is sufficient for the reservoir to be assumed infinite. This has been checked using a larger reservoir ($7\,\mathrm{cm} \times 15\,\mathrm{cm}$), where the capillary rise height was found to be similar to that of the smaller one.

## Colloidal suspensions

Commercial suspensions of silica colloids in water have been used (50R50 Klebosol from AZ materials). They are 52.7 wt%, and the silica particles have a density of 2.16. These silica particles are spherical and have a mean diameter of 76 nm, as checked by atomic force microscopy (AFM), and are rather monodisperse. They exhibit a standard deviation of about 4 nm in diameter. The 52.7% initial solution has been diluted using pure water to vary the weight fraction. Note that the suspension used are very stable, no agglomeration or precipitation is observed even after 1 year.

## Glass cleaning

The commercial glass plates are cleaned during 15 to 30 minutes in a hot mixture of concentrated sulfuric acid (98%) and hydrogen peroxyde (50% water solution), in 70/30 proportions. Then they are rinsed many times in pure water before being dried using a nitrogen flow. Just after this cleaning procedure, the glass slides exhibit a total wetting by water. However, after several minutes, water only partially wets the surfaces, with a receding contact angle that is about 10 degrees. Such an effect is probably due to uncontrolled contamination of the surface. In order to ensure that the contact angle remains at similar values for all the experiments, the glass slides are always used 15 minutes after the cleaning procedure. They exhibit a contact angle hysteresis that is rather important, advancing contact angle is about $20^\circ$.

## Contact line displacement

The position of the capillary rise is governed through the emptying of the reservoir, achieved using a syringe pump (Pumping system: Kd Scientific ; Syringe: 60ml Maximum). The accessible range of flow rates allows us to explore a contact line velocity range lying between a few nanometers per second up to 2mm/s. For all experiments, the tank is emptied out with a constant pumping rate. For pure water, this protocol corresponds to a constant contact line velocity $V$ and then to a linear decreasing of the capillary rise height.

The position of the meniscus that is on the top of the capillary rise is monitored during the experiment. For that purpose we acquire images at regular intervals with a AVT Marlin F131B digital camera, having a resolution of $1280 \times 1024$ pixels. The position of the meniscus is then determined with a subpixel analysis of the images which leads to a precision of the order of 2 $\mu$m.

## Evaporation control

The experiments are inside a 25L chamber, where temperature and humidity are controlled. The humidity could be varied from 15 to 95%, using either an air flow through a dissecant either a moist air flow. The temperature could be raised up to 70°C.

A vertical air flow is blown between the two glass plates. A fan is placed on the top of a rectangular channel whose cross section matches the two glass slides. The channel is 10 cm high. The velocity was chosen to get a uniform flow close to the meniscus but a negligible interface deformation due to the pressure increase above the meniscus.

To get the evaporation flux corresponding to the different experimental conditions (air flow, temperature, humidity), previous experiments were performed with pure water by cutting the connection between the plates and the reservoir and measuring the decrease of the water level between the two plates. These measurements were made using pure water. Three temperature set points have been used and lead to the following values: $v_{\text{evap}} = 0.4\mu\text{m.s}^{-1}$, $1\mu\text{m.s}^{-1}$ and $1.95\mu\text{m.s}^{-1}$ for temperatures in the chamber of 25°C, 50°C and 70°C respectively.

## Experimental procedure

The glass plates are placed inside the environmental chamber just after the cleaning procedure, 15 minutes before the beginning of every experiments, so that thermal and humidity equilibrium is achieved. Then, the plates are immersed deeply in the reservoir and the air flow is turned on. About 5 minutes later, when we can assume that evaporation has reached its steady state, the level of the reservoir is quickly lowered of a few millimeters for two reasons. First, when observing a posteriori the plates, it allows to distinguish the beginning of the experiment from the first deposition that has settled during the 5 minutes of first immersion. Second, it ensures that the contact angle has reached the receding value. All the experiments reported in this article concern receding contact angles.

# Results and discussion

## Coating regimes

Several coating regimes can be observed when varying the contact line velocity of the colloidal suspension under study. For given particle volume fraction and evaporation rate, and for velocities up to 1 mm/s, one observes successively:

(i) For very low velocities, a strong stick-slip motion of the contact line is observed. An example of the contact line motion in this regime is shown in Figure 2B. It leads to very regular patterns that are parallel to the contact line. Their height is on the order of a few microns. Between each deposit, there is an area free of particles or with one particle layer. The profilometer image shown in Figure 3A illustrates this deposition regime. The wavelength is rather high (200$\mu$m to 1mm).

(ii) For intermediate velocities, the stick-slip motion of the contact line is less pronounced and smooth oscillations are observed (see Figure 2A). Correlatively, the pattern height is smaller, it decreases to a few layers of particles. The pattern wavelength is also smaller (50-200 $\mu$m).

(iii) At high velocities, the contact line velocity is steady and the resulting coating is isotropic. It is homogeneous at large scale. Particles are randomly dispersed or arranged in small areas. Images showing such isotropic depositions could be found in our previous communication.[9]

In Figure 3B, an optical image of a glass slide coated under successive increasing velocities illustrates these qualitative regimes. The transition velocities depend significatively on the particle volume fraction and on the evaporation rate. They are not well established since it seems difficult to define unambiguous criteria. Indeed, as could be seen in the optical image in Figure 3, the transition from periodical patterns to uniform deposition is not sharp. As the velocity increases, the pattern amplitude decreases and progressively looses its regularity.

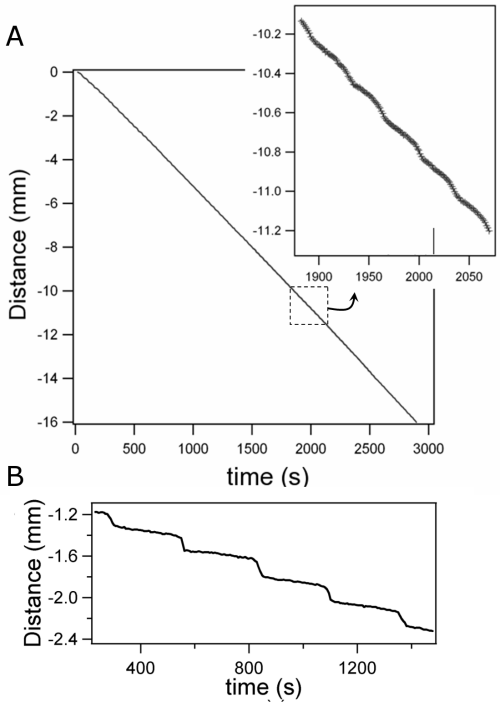


Figure 2: Examples of the meniscus displacement obtained by the analysis of the images. - A. The imposed average velocity is 5.5 $\mu$m/s, temperature 25°C, humidity 30%, $v_{\text{evap}} = 0.4\mu\text{m.s}^{-1}$, and the suspension volume fraction is 2.9%. The insert is a zoom on a small portion of this displacement showing the periodic deviations of the contact line from the imposed position. - B. Strong stick-slip at 0.95$\mu$m/s with a volume fraction of 1.4%.

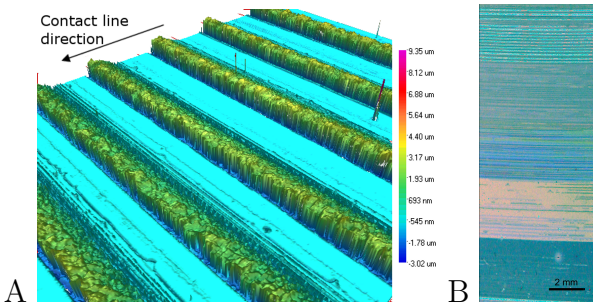


Figure 3: A. Optical profilometer image of a periodic deposit obtained in the following conditions: imposed average velocity = 1 $\mu$m/s, particle volume fraction = 1.41%, hummidity 90%, $T = 25$°C, $v_{\text{evap}} \simeq 0.06\mu$m/s. The image dimensions are 1447×1092 $\mu$m, and the typical pattern height is 5$\mu$m. - B. Optical image of a dried glass slide. The image is taken at 45° of the normal direction in order to enhance the colors, which are linked to the thickness of the deposit layer. Different velocities have been imposed during this experiment. Starting from the top, these were 2.8, 5, 8, 15 and 25 $\mu$m/s. For the lowest velocities a macroscopic periodical pattern is observed whereas for the fastest ones the uniformity of the color indicates that the deposit is uniform. The volume fraction was 2.9%, the temperature 25°C, the humidity 30%, and $v_{\text{evap}} = 0.4\mu\text{m.s}^{-1}$.

Atomic force microscopy and electronic microscopy characterizations of the smallest patterns reveal that the uniform deposition correspond to only 1 or 2 layers of particles. Correlatively, the smallest regular patterns height is about 1 to 3 layers. These observations indicate that the stick-slip regime at low velocities holds as soon as the pattern height is bigger than the particle size.

This article focuses on the periodical patterns regime obtained at low and intermediate velocities, that is to say when the oscillations of the contact line motion are higher than the measurement uncertainty (2 $\mu$m).

## Stick/slip regime - Pinning force

Figure 2 shows an example of the contact line position as a function of time for the stick/slip regime. Its average position follows the displacement of the reservoir liquid level, but exhibits periodic deviations around the linear imposed variation. It has been checked that the pumping rate is constant. Indeed, for pure water, such deviations are not observed. This allows us to conclude that the periodic variations of the meniscus position are due to an interaction between the contact line and the deposit that is formed on the glass substrate.

For the geometry used in the experiments, the energy of the system reads

$$E = -2\gamma h \cos\theta + \frac{1}{2}\rho g e h^2, \tag{1}$$

where $\gamma$ is the liquid surface tension, $\theta$ is the contact angle between the liquid and the vertical clean glass plate, $\rho$ the density and $g$ the gravity.[33] The equilibrium capillary rise height $h$ corresponds to the minimum of the energy (Jurin's law):

$$h = \frac{2\gamma \cos\theta}{\rho g e}, \tag{2}$$

.

The presence of a deposit can change this height by a given quantity $\Delta h$ and in the limit

of low velocities this deviation reflects a pinning force that is acting on the two contact lines of the deposit, given for each contact line by:

$$f = \gamma \left(\cos\theta - \cos\theta_0\right) = \frac{1}{2}\rho g e \Delta h, \tag{3}$$

where $\theta_0$ is the contact angle in absence of deposit.

An implicit assumption here and in the following is that the pinning force, which is in principle a local quantity, is constant along the contact line. Thus, as a first approximation, the problem could be considered as two-dimensional. This assumption is consistent with experimental observations that always show patterns parallel to the contact line (cf. Figure 3).

Another assumption in the analysis is that the system is at static equilibrium; i.e., the viscous force could be neglected. Indeed, the capillary numbers remains below $10^{-5}$. Even though viscous stresses may slightly modify the apparent contact angle at these capillary numbers,[34] the effect is small enough to be neglected. Evaporation itself also modifies the apparent contact angle, but at these small velocity and with moderate evaporation rate, this effect could also be neglected.[35,36]

During the pinning, the contact line velocity $V$ is smaller than the velocity imposed by the pumping rate (see Figure 2). Then the unpinning occurs and the contact line velocity becomes larger than $V$. The phenomenon is time periodic of period $\tau$. Using equation 3 the deviations of the capillary rise $\Delta h$ lead to a direct measurement of the pinning force acting on the contact line. Some examples of the resulting pinning force as a function of time are shown in Figure 4. When the velocity $V$ is small, this pinning force increases up to a maximal value called thereafter $f_{\max}$, before it quickly relaxes to zero. This correspond to a strong pinning, since the contact line velocity is small during the pinning as compared to the velocity imposed by the pumping rate. The pinning time $t_p$ is much larger than the unpinning one. For higher velocities, the pinning is still time periodic but weaker. The

maximal pinning force $f_{\max}$ is defined as the amplitude of the oscillations, similarly to strong pinning case, where its definition is straightforward. In that case the pining and unpinning times are of the same order. These behaviors have been observed for all the experiments performed, i.e. the pinning time $t_p$ is of the order or much larger than the unpinning one, so that we get the following order of magnitude $t_p \sim \tau$. Again, no sharp transition between a stick-slip regime towards a steady one is observed, since the lowest oscillatory pinning forces observed fall below the precision of the measurement. The uniform deposition that is achieved at high velocities seems to be the limit of a vanishing maximal pinning force.

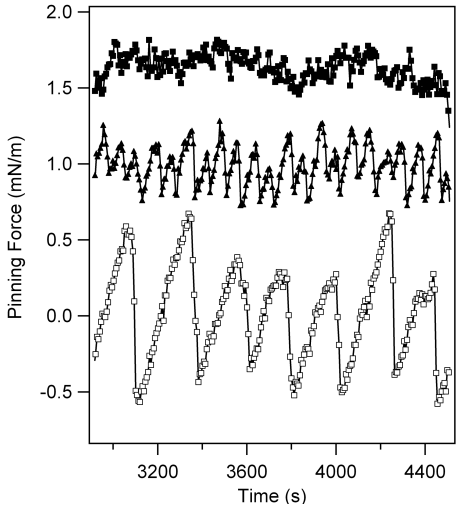


Figure 4: Examples of pinning force measurements. The data have been horizontally displaced for clarity. From the top to the bottom the corresponding imposed velocities are 20, 9 and 3.5 $\mu$m/s. The weight fraction is 16%, temperature 25°C, humidity 30% and $v_{\text{evap}} = 0.4\mu\text{m.s}^{-1}$.

## Scaling laws for the pinning force

The experimental conditions are varied systematically and we focus on the amplitude $f_{\max}$ of the pinning force. This amplitude is defined as the value of the pinning force just before the unpinning occurs. Figure 5 shows the results obtained with different particles volume fraction $\phi$. The pinning force decreases when increasing the velocity and it increases when increasing the concentration. An empirical law is found and is shown in the inset in Figure 5.

The amplitude of the pinning force is given in the studied regime by $f_{\max}/\gamma = 5.9 \cdot 10^{-7}\phi/V$, where $V$ is the imposed velocity and $\gamma$ the water surface tension.

Then the evaporation rate has been varied. The higher it is, the higher the amplitude of the pinning force. As shown in Figure 6, the data collapse on a single line when the velocity is normalized by the evaporation rate. Thus it indicates that the following law is observed:

$$\frac{f_{\max}}{\gamma} = 1.4\phi\frac{v_{\text{evap}}}{V} \tag{4}$$

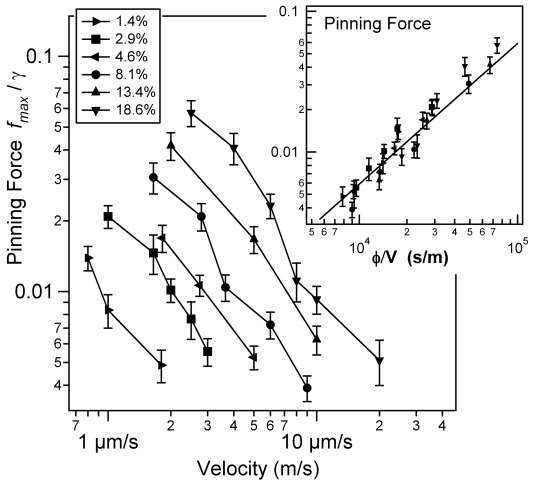


Figure 5: Maximum pinning force $f_{max}$, normalized by the surface tension of water at 25° (71.9 mN/m) as a function of the imposed velocity, for various particle volume fraction ranging between 0.014 and 0.19 (see the legend). Temperature is 25°C, humidity is 30%. $f_{max}$ is determined from in situ measurement of the contact line position, as shown in Figure 4, averaged on about or over 20 periods. The error bars represent the standard deviation calculated on this set of data. In insert, the same data are plotted versus $\phi/V$, which is the empirical scaling suggested by the data. The solid line corresponds to the best linear fit to the data weighted by the inverse of their standard deviation, and the following empirical law is obtained: $f_{max} \simeq 5.9 \cdot 10^{-7}\phi/V$.

## Pinning force and deposit volume

Let us discuss the kinetics of the growth of the deposit and its correlation with the pinning force.

Some recent experimental results brought evidence that particle deposition at low contact

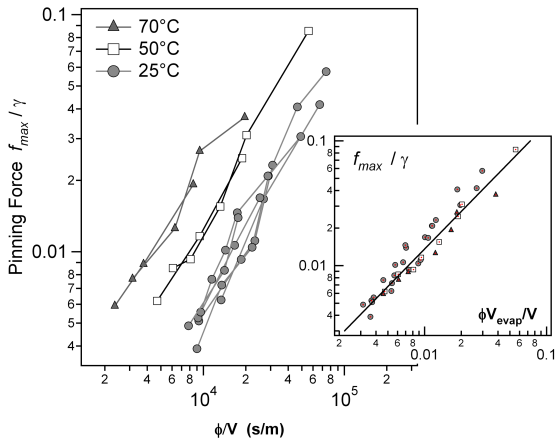


Figure 6: Amplitude of the dimensionless pinning force $f_{max}/\gamma$ for various velocities $V$, particle volume fractions $\phi$ and 3 different temperatures (25, 50 and 70°C), using for the water surface tension the following values : 71.9, 67.8, and 64.5 mN/m, respectively. It is plotted as a function of $\phi/V$. In insert, the same data are plotted as a function of $\phi \cdot v_{\rm evap}/V$. That is to say the velocity is normalized by the evaporation rate. The solid line corresponds to the best linear fit to the data weighted by the inverse of their standard deviation, and the following prefactor is obtained $f_{max}/\gamma \simeq 1.4\,\phi\, v_{\rm evap}\,/\,V$.

line velocities is mainly driven by evaporation. Indeed, Le Berre *et al*[8] and us[9] reported that the mean thickness of the deposit could be accounted by a simple mass balance, involving the evaporation flux $Q_{ev} = Lv_{\rm evap}$, with the scale length $L$ being on the order of the meniscus size. This simple model accounts that the deposit thickness scales as 1/V. It implies that the deposition rate is constant when varying the velocity in the evaporative regime, and is given by $\phi L v_{\rm evap}$.[9] This has been shown on different systems for various experimental conditions, and holds for the velocity range of the experiments reported in this article, that is to say velocities typically lower than 100 $\mu$m/s at room temperature. In the stick-slip regime, we thus expect that the constant deposition rate $\phi L v_{\rm evap}$ holds, and, that the volume of one pattern is given by $\phi L v_{\rm evap} t_p$, where the pinning time $t_p$ is the time elapsed between the beginning of the pinning and the unpinning event.

Let us furthermore make the hypothesis that the pinning force is a unique function of the deposit volume, independently on the deposition rate. Under these assumptions, it should be a function of the quantity $\phi L v_{\rm evap} t_p$ only. In Figure 7, the normalized pinning force measured in various conditions is plotted as a function of $\phi L v_{evap} \tau$, where $\tau$ is the period

of the stick-slip motion, which is an estimate of $t_p$ as described in the previous section. All points obviously gather on a single curve, which is well approximated by a 1/2 power-law. More precisely, it is found to be given by the empirical expression

$$f_{\max} \simeq C\gamma\sqrt{\phi L v_{\text{evap}}\tau}, \tag{5}$$

with $C = 250\,\text{m}^{-1}$. This results justifies the assumptions made, that are: the deposit formation is independent on the velocity, the pinning force is a unique function of its volume.

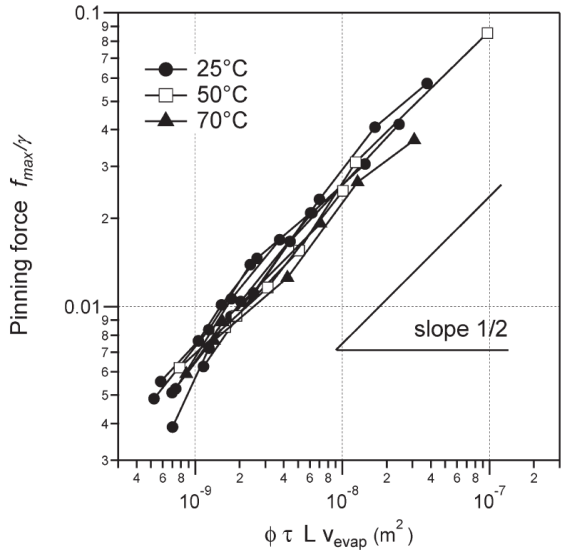


Figure 7: Dimensionless pinning force (same data as Figure 6) for various expriments, plotted as a function of $\phi L v_{\text{evap}}\tau$, where $\tau$ is the period of the stick-slip motion of the contact line, and $L = 0.5$ mm is half the thickness of the cell.

This result is empirical. However, we should notice that it is consistent with the scaling law reported in the previous section and summarized in equation 4. Indeed, in the limit of perfect pinning, the contact line displacement during the pinning is negligible and the maximal pinning force is $f_{\max} = \rho g e V t_p/2$. Actually the contact line moves slowly during the pinning but its displacement during the pinning is always smaller than during the unpinning, so that, in order of magnitude and in a first approximation, this relation may be applied to our experiments. The maximal pinning force that the deposit could support is given by $f_{\max} \simeq C\gamma\sqrt{\phi L v_{\text{evap}} t_p}$, according to equation 5. The elimination of the pinning time in these

equations leads to $f_{\max} \sim \phi v_{\text{evap}}/V$, which is the scaling reported in Figure 6, observed by measuring the pinning force in various experimental conditions.

One may notice that the pinning force grows proportionally to $\sqrt{t}$ (see equation 5) while the force due to gravity (deviation from the equilibrium position of the contact line) increases linearly with respect to the pinning time. The pinning/unpinning results of the competition between theses two forces and the difference in the growth rate is a necessary condition to observe a stick-slip motion and correlatively a horizontal patterning of the surface.

Let us finally link these results to our previous work where the origin of the pinning force was discussed.[32] In this paper the maximum pinning force $f_{\max}$, measured in situ by image analysis, has been correlated to the tilt of the deposit $\partial_x \xi$ (see Figure 8), measured a posteriori by AFM profile. It was found that $f_{\max} \simeq \gamma \sin\theta_0 \partial_x \xi$. This result supports the interpretation that the pinning force is due to the geometry of the patterns - let us recall that we have used silica particles that are chemically quite similar to the glass substrate so that no strong modification of the surface free energy is expected -. Assuming this interpretation of the pinning, the above conclusions for the pinning force apply directly to the slope of the deposit. For a given deposit volume $\mathcal{V}$, the results reported in the present paper indicate that the characteristic slope responsible for the pinning is proportional to $\mathcal{V}^{1/2}$. The geometry of the deposit thus depends only on its volume, and, more precisely, $\partial_x \xi \propto \sqrt{\phi v_{\text{evap}} t_p}$. Further experiments should be needed to confirm this result but fall out of the scope of this work.

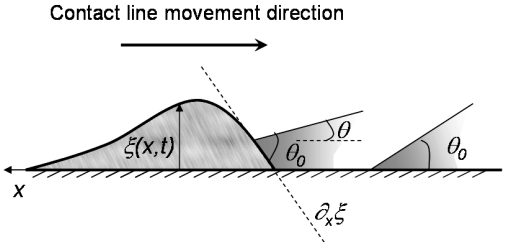


Figure 8: Schematic representation of the geometric pinning of a contact line on a deposit. The height of the deposit being $\xi(x)$, the equilibrium angle $\theta$ of the contact line with respect to the flat surface is given by $\theta_0 - \arctan \partial_x \xi$.

# Conclusion

The coupling between particles deposition induced by evaporation and contact line velocity has been investigated when the concentration, the evaporation rate and the velocity are varied. We report some experimental results that describe a successive pinned-unpinned motion of the contact line of a colloidal suspension under evaporation. Some simple scaling laws have been found to describe well the amplitude of the stick-slip phenomenon. Our analysis of the experimental results supports the idea that the pinning force is a unique function of the deposit volume, which is simply the deposition rate times the pinning time. The velocity of the contact line has, however, a great influence on the pinning time, and could thus be used to control the wavelength of the patterns.

Interesting future work would be to test whether these results depend on the material and on the substrate. This should provide data that could help in drawing a comprehensive picture of the stick-slip motion induced by the evaporation of the contact line.

# Acknowledgement

This work has been supported by the ANR DESPEC 05-BLAN-0056-01 for fundings. The authors thank F. Lequeux and L. Limat for fruitful discussions.

# References

(1) Rio, E.; Daerr, A.; Lequeux, F.; Limat, L. Moving contact lines of a colloidal suspension in the presence of drying. *Langmuir* **2006**, *22*, 3186–3191.

(2) Abkarian, M.; Nunes, J.; Stone, H. A. Colloidal crystallization and banding in a cylindrical geometry. *J. Am. Chem. Soc.* **2004**, *126*, 5978–5979.

(3) Ray, M. A.; Kim, H.; Jia, L. Dynamic self-assembly of polymer colloids to form linear patterns. *Langmuir* **2005**, *21*, 4786–4789.

(4) Xu, J.; Xia, J. F.; Hong, S. W.; Lin, Z. Q.; Qiu, F.; Yang, Y. L. Self-assembly of gradient concentric rings via solvent evaporation from a capillary bridge. *Phys. Rev. Lett.* **2006**, *96*, 066104.

(5) Small, W. R.; Walton, C. D.; Loos, J.; Panhuis, M. I. H. Carbon nanotube network formation from evaporating sessile drops. *J. Phys. Chem. B* **2006**, *110*, 13029–13036.

(6) Byun, M.; Hong, S. W.; Zhu, L.; Lin, Z. Q. Self-assembling semicrystalline polymer into highly ordered, microscopic concentric rings by evaporation. *Langmuir* **2008**, *24*, 3525–3531.

(7) Monteux, C.; Elmaallem, Y.; Narita, T.; Lequeux, F. Advancing-drying droplets of polymer solutions: Local increase of the viscosity at the contact line. *Epl* **2008**, *83*, 34005.

(8) Berre, M. L.; Chen, Y.; Baigl, D. From Convective Assembly to Landau-Levich Deposition of Multilayered Phospholipid Films of Controlled Thickness. *Langmuir* **2009**, *25*, 2554–2557.

(9) Jing, G.; Bodiguel, H.; Doumenc, F.; Sultan, E.; Guerrier, B. Drying of Colloidal Suspensions and Polymer Solutions near the Contact Line: Deposit Thickness at Low Capillary Number. *Langmuir* **2010**, *26*, 2288–2293.

(10) Fan, F. Q.; Stebe, K. J. Assembly of colloidal particles by evaporation on surfaces with patterned hydrophobicity. *Langmuir* **2004**, *20*, 3062–3067.

(11) Vyawahare, S.; Craig, K. M.; Scherer, A. Patterning lines by capillary flows. *Nano Letters* **2006**, *6*, 271–276.

(12) Helseth, L. E.; Fischer, T. M. Particle interactions near the contact line in liquid drops. *Phys. Rev. E* **2003**, *68*, 051403.

(13) Yarin, A. L.; Szczech, J. B.; Megaridis, C. M.; Zhang, J.; Gamota, D. R. Lines of dense nanoparticle colloidal suspensions evaporating on a flat surface: Formation of non-uniform dried deposits. *J. Coll. Inter. Sci.* **2006**, *294*, 343–354.

(14) Deegan, R. D.; Bakajin, O.; Dupont, T. F.; Huber, G.; Nagel, S. R.; Witten, T. A. Capillary flow as the cause of ring stains from dried liquid drops. *Nature* **1997**, *389*, 827–829.

(15) Hu, H.; Larson, R. G. Marangoni effect reverses coffee-ring depositions. *J. Phys. Chem. B* **2006**, *110*, 7090–7094.

(16) Ristenpart, W. D.; Kim, P. G.; Domingues, C.; Wan, J.; Stone, H. A. Influence of substrate conductivity on circulation reversal in evaporating drops. *Phys. Rev. Lett.* **2007**, *99*, 234502.

(17) Harris, D. J.; Lewis, J. A. Marangoni effects on evaporative lithographic patterning of colloidal films. *Langmuir* **2008**, *24*, 3681–3685.

(18) Adachi, E.; Dimitrov, A. S.; Nagayama, K. Stripe Patterns Formed on A Glass-Surface During Droplet Evaporation. *Langmuir* **1995**, *11*, 1057–1060.

(19) Chon, C. H.; Paik, S.; Tipton, J. B.; Kihm, K. D. Effect of nanoparticle sizes and number densities on the evaporation and dryout characteristics for strongly pinned nanofluid droplets. *Langmuir* **2007**, *23*, 2953–2960.

(20) Govor, L. V.; Reiter, G.; Bauer, G. H.; Parisi, J. Nanoparticle ring formation in evaporating micron-size droplets. *Appl. Phys. Lett.* **2004**, *84*, 4774–4776.

(21) Younes-Metzler, O.; Ben, R. N.; Giorgi, J. B. Pattern formation of antifreeze glycoproteins via solvent evaporation. *Langmuir* **2007**, *23*, 11355–11359.

(22) Kuncicky, D. M.; Velev, O. D. Surface-guided templating of particle assemblies inside drying sessile droplets. *Langmuir* **2008**, *24*, 1371–1380.

(23) Kajiya, T.; Kaneko, D.; Doi, M. Dynamical Visualization of "Coffee Stain Phenomenon" in Droplets of Polymer Solution via Fluorescent Microscopy. *Langmuir* **2008**, *24*, 12369–12374.

(24) Petsi, A. J.; Burganos, V. N. Evaporation-induced flow in an inviscid liquid line at any contact angle. *Phys. Rev. E* **2006**, *73*, 041201.

(25) Popov, Y. O.; Witten, T. A. Characteristic angles in the wetting of an angular region: Deposit growth. *Phys. Rev. E* **2003**, *68*, 036306.

(26) Popov, Y. O. Evaporative deposition patterns: Spatial dimensions of the deposit. *Phys. Rev. E* **2005**, *71*, 036313.

(27) Zheng, R. A study of the evaporative deposition process: Pipes and truncated transport dynamics. *Eur. Phys. J. E* **2009**, *29*, 205–218.

(28) Witten, T. A. Robust fadeout profile of an evaporation stain. *Epl* **2009**, *86*, 64002.

(29) Ghosh, M.; Fan, F. Q.; Stebe, K. J. Spontaneous pattern formation by dip coating of colloidal suspensions on homogeneous surfaces. *Langmuir* **2007**, *23*, 2180–2183.

(30) Diao, J. J.; Sun, J. W.; Hutchison, J. B.; Reeves, M. E. Self assembled nanoparticle wires by discontinuous vertical colloidal deposition. *Appl. Phys. Lett.* **2005**, *87*, 103113.

(31) Diao, J. J.; Hutchison, J. B.; Luo, G. H.; Reeves, M. E. Theoretical analysis of vertical colloidal deposition. *J. Chem. Phys.* **2005**, *122*, 184710.

(32) Bodiguel, H.; Doumenc, F.; Guerrier, B. Pattern formation during the drying of a colloidal suspension. *Eur. Phys. J. ST* **2009**, *166*, 29–32.

(33) De Gennes, P.-G.; Brochard-Wyart, F.; Quere, D. *Capillary and Wetting Phenomena : Drops, Bubbles, Pearls, Waves.*; Springer, 2003.

(34) Huh, C.; Scriven, L. E. Hydrodynamic Model of Steady Movement of A Solid/Liquid/Fluid Contact Line. *J. Coll. Inter. Sci.* **1971**, *35*, 85.

(35) Berteloot, G.; Pham, C. T.; Daerr, A.; Lequeux, F.; Limat, L. Evaporation-induced flow near a contact line: Consequences on coating and contact angle. *Epl* **2008**, *83*, 14003.

(36) Butt, H. J.; Golovko, D. S.; Bonaccurso, E. On the derivation of Young's equation for sessile drops: Nonequilibrium effects due to evaporation. *J. Phys. Chem. B* **2007**, *111*, 5277–5283.

# For Table of Contents Use Only